IEEE Access
Multidisciplinary | Rapid Review | Open Access Journal

Received September 19, 2017, accepted November 21, 2017, date of publication November 24, 2017,
date of current version February 14, 2018.

Digital Object Identifier 10.1109/ACCESS.2017.2777521

A Porous Scaffold Design Method for Bone Tissue Engineering Using Triply Periodic Minimal Surfaces

JIANPING SHI[1,2], JIQUAN YANG[2], LIYA ZHU[2], LAN LI[1], ZONGAN LI[2], AND XINGSONG WANG[1]

[1]School of Mechanical Engineering, Southeast University, Nanjing 210096, China
[2]Jiangsu Key Laboratory of 3-D Printing Equipment and Manufacturing, Nanjing Normal University, Nanjing 210042, China

Corresponding author: Xingsong Wang (xswang@seu.edu.cn)

This work was supported in part by the Post-Doctoral Science Foundation of Jiangsu province under Grant 1601010B, in part by the Key Technology Research and Development Program of Jiangsu province under Grant BE2016010, in part by the National Natural Science Foundation of China under Grant 61273243 and Grant 51407095, in part by the Natural Science Foundation of Jiangsu province under Grant BK20150973, in part by the Scientific Research Innovation Program for Graduate of Jiangsu province under Grant SJLX16_0282, and in part by the Science and Technology Achievement Transformation Foundation of Jiangsu province under Grant BA2016106.

ABSTRACT Among the various scaffold design methods, function-based modeling is of great interest due to its accurate controllability for designing pore architectures. Parameters, such as the pore size, pore shape, porosity, and channel interconnectivity, should be designed according to actual skeleton characteristics. To this, an effective modeling method of trabecular bone is proposed, combining triply periodic minimal surface (TPMS) and fractal geometry. First, the surface morphology of real trabecular bone is obtained based on the binary processing of computed tomography images. Then, the fractal pore-making element using TPMS is built and constructed into a complex porous structure. Finally, the customized scaffold model is manufactured with an additive manufacturing method.

INDEX TERMS Bone tissue, TPMS, porous scaffold, 3D printing.

I. INTRODUCTION

Bone tissue engineering is a comprehensive subject that uses biotechnology and biomaterials to replace or repair damaged human bone tissues. With respect to bone tissue engineering, a bionic scaffold is a near substitute for bone structure and function. The bionic scaffold should not only have the functional characteristics of compact and cancellous bone but also have the structural features of the Haversian canal and the Volkmann canal [1]. In other words, to construct tissue-engineered bone, the bionic scaffold must provide the required mechanical support for the new bone tissue and provide the appropriate micro space for the adhesion and proliferation of bone cells. In addition, the micro pores within the scaffold must be interconnected to provide suitable nutrient channels for the bone cells to guide the formation and maturation of new bone cells [2]–[4].

During the research process for the porous scaffold fabrication, we uncovered many ways to prepare scaffolds, including particulate leaching, gas foaming, fiber bonding, and phase separation [5]. The properties of these scaffolds are different with different preparation methods. Moreover, the function of the newly constructed tissue will be affected by the processing quality of the scaffold. In addition, these traditional methods are more committed to the construction of the internal pore structure, and the anatomical shape of the scaffold mainly relies on handcrafting or molding. As a result, a complex anatomical structure that accurately matches the defect area is impossible to produce. In addition, the porosity, connectivity and uniformity of the micro pore structure cannot be evaluated prior to the fabrication, and the manufacturing process is also difficult to control [6].

Due to difficultly in controlling the pore characteristics (including pore size, pore shape, and pore size distribution) of bone scaffolds, it is difficult to meet the requirements of bionic bone tissue fabrication with these traditional methods. The development of three-dimensional printing technology has solved this problem, and it has shown great advantages in the fabrication of porous bone scaffold that meets the individual requirements [7], [8]. Through the technology, a series of level data is decomposed from the 3D model for direct

manufacturing the bone scaffold. The model is accumulated from point to plane and then the body. While obtaining the macro structure of the bone scaffold, it can also control its micro topological structure to a certain extent [12].

The establishment of the bone tissue engineering scaffold model with functional and morphological features close to the true pore features of the skeleton is the prerequisite for the successful preparation of bone scaffolds. The micro pore characteristics of natural bone (such as surface morphology and pore size distribution) are complex and irregular [13]. At present, the scaffold modeling method mainly includes an image-based method, a CAD method, an implicit surface method and so on. The image-based method is a reverse engineering technology. It is difficult to guarantee the connectivity of the pores in this method because the bones are considered as slices and are designed layer by layer. The CAD method is suitable for modeling porous structures with simple rules. Implicit surface modeling has unique advantages for large and complex topological structures with large spatial distortions [14]. The current bone scaffold modeling of the hole is a regular structure. It is difficult to carry out an effective description of the complexity and irregularly of the natural bone tissue structure. Achieving effective control of the micro structure is not possible, so it is difficult to create a completely model in accord with bone scaffold demand [15].

To solve this problem, the Micro-CT (micro computed tomography) data of the nature bone tissue is acquired and analyzed in this paper. Based on the analysis of bone tissue morphology [16]–[18], a modeling method for the microstructure of bone scaffold was proposed based on a triply periodic minimal surface TPMS [19]–[25], which can effectively describe the surface morphology and pore size distribution of the bone microstructure.

II. MICRO-CT DATA PROCESSING METHOD

The B6 rat femur was employed as the object of research in this paper, and the samples were scanned by SkyScan 1076 Micro-CT (Bruker Micro-CT, Belgium) to obtain the two-dimensional stratified micro-CT data of the samples. The obtained images are two-dimensional grayscale diagrams that contain the basic information on the solid parts and the inner pores of the sample, as shown in Fig. 1(a). The process of image processing is mainly the binarization of the image. The binary processing is to extract the information on the hole and solid in a 2D gray image. By adjusting the gray threshold, the proportion of the image with the porous feature is basically the same as the structure of the bone sample, and then the gray value can be used as the two-phase distinguishing critical threshold.

To maintain the accuracy of the segmentation image, partial volume effects should be considered to select the accuracy of the threshold [26]. Under the influence of the partial volume effect, the gradient amplitude of some trabecular bone does not coincide with the threshold segmentation boundary when the gradient amplitude of a size trabecular bone coincides with the boundary of the threshold segmentation.

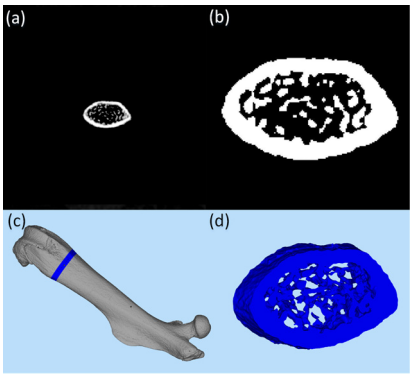

FIGURE 1. Micro-CT processing of B6 rat femur: (a) CT image of the femur; (b) image processed by binarization; (c) 3D model of the femur reconstructed by MINICS; (d) a section of the femur.

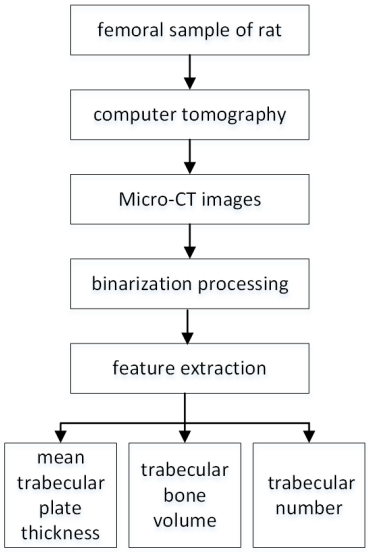

FIGURE 2. Progress of obtaining the geometric characteristics of trabecular bone.

In determining the threshold, the trabecular bone size range should be determined first compared to the standard, then compared with the size of the gradient of trabecular bone. The best threshold was identified as the image segmentation threshold, and the cancellous bone is further divided into trabecular bone and bone marrow cavity, as shown in Fig. 1(b).

A. GEOMETRIC CHARACTERISTICS OF TRABECULAR BONE

Through the binarization processing of the trabecular bone CT image, we can obtain the following three geometric feature factors: MTPT (mean trabecular plate thickness), TBV (trabecular bone volume) and TN (trabecular number) [27]. The description of these parameters can be used for the quantitative analysis of bone morphometry. The progress of obtaining the geometric characteristics of trabecular bone is shown in Fig. 2.

In the calculation of the mean trabecular thickness, it refers to the average thickness of bone sections of the trabecular

TABLE 1. Geometric features of the average of the calculated value of trabecular bone in mouse femur.

Model	number of trabecular bone	mean trabecular plate thickness	trabecular bone volume
Mouse femur	15±2	56.40μm	14.83%

wall. The section of the trabecular bone can be considered an approximately irregular ring. For the ring, the outer diameter is D, and the inner diameter is d. The thickness of the ring can be expressed by $(D-d)/2$. The area of the ring (S) is divided by the sum of the inside and outside circumference (C), it is available in formula (1):

$$\frac{S}{C} = \frac{\pi D^2 - \pi d^2}{2\pi D + 2\pi d} = \frac{D-d}{2} \tag{1}$$

The average trabecular bone thickness is approximated by formula (2):

$$MTPT = \frac{S}{C} \tag{2}$$

By combining the ratio of the image to the object, the approximate thickness of the actual trabecular bone can be calculated.

The trabecular bone volume refers to the volume fraction of trabecular bone and all bone marrow cavity. The bone marrow cavity and the trabecular bone in the slice are approximately regarded as cylinders. The calculation formula of the trabecular bone volume is shown in formula (3):

$$TBV = \frac{V_1}{V_2} \tag{3}$$

Where, V_1 refers to the measured trabecular volume, and V_2 refers to the measured bone marrow cavity volume.

The trabecular number is another factor to describe the form feature of the trabecular bone shape. Based on the idea of labeling the connected domain in an image, the number of the trabecular bone is calculated and the centroid is labeled. This method can intuitively and rapidly realize the statistics of the number of trabecular bone.

According to the parameter calculation above, the trabecular number, mean trabecular plate thickness and trabecular bone volume were calculated and are shown in Table 1.

B. DISTRIBUTION CHARACTERISTICS OF TRABECULAR BONE

The regional distribution of information on trabecular bone acquisition is the key point of analysis of the internal structure of bone. In this study, the spatial distribution of the trabecular bone is analyzed based on the gray co-occurrence matrix of the region texture description [28], [29]. The four parameters, contrast, entropy, angular second moment, and correlation, are chosen as the factors describing the change of the region.

Contrast (C) reflects the influence of texture clarity. The visual effect of image is clearer with the deeper texture of the groove. Conversely, the contrast decreases with the more blurred in the vision. The formula for the contrast is shown in formula (4):

$$\mathrm{C} = \sum_{N=0}^{L-1} n^2 \left\{ \sum_{i=0}^{L-1} \sum_{j=0}^{L-1} P(i,j) \right\} \tag{4}$$

where L is the number of gray levels.

Entropy (H) is the measurement of the amount of information that an image has. The entropy value is close to zero as the image does not have any texture. Otherwise, if the image is full of fine texture, the entropy value of the image is the largest. The formula for entropy is shown in formula (5):

$$\mathrm{H} = -\sum_{i=0}^{L-1} \sum_{j=0}^{L-1} P(i,j) \log P(i,j) \tag{5}$$

The angular second moment (E) is also known as energy, and the angular second moment reflects the uniformity of image gray distribution. The energy moment of coarse texture is larger, while the energy moment of fine texture is smaller. The angular second moment can be expressed by formula (6):

$$\mathrm{E} = -\sum_{i=0}^{L-1} \sum_{j=0}^{L-1} P(i,j)^2 \tag{6}$$

Relevance (C_{rl}) is a linear dependence of the field that can be expressed by formula (7):

$$\mathrm{C}_{rl} = -\sum_{i=0}^{L-1} \sum_{j=0}^{L-1} \frac{ijP(i,j) - u_1 u_2}{\sigma_1^2 \sigma_2^2} \tag{7}$$

According to the parameter calculation above, the values of contrast, entropy, energy, and correlation are shown in Table 2.

TABLE 2. Image feature parameters of trabecular in mouse femur.

Model	contrast	entropy	energy	relevance
Mouse femur	0.0154	0.2762	0.8636	0.8205

To understand the specific spatial distribution of voids in specimens, the whole coordinates of CT scanning images were extracted using the analytical software MINICS (Materialise, Belgium), as shown in Fig. 1(cd). The size and distribution of the pores in the specimens were statistically analyzed. According to the analysis of the pore structure in the software, the porosity of the rat femoral truncated sample is 70.52%.

A bone scaffold 3D model can be established by a CT image reversing technique. The method simulates the microstructure close to the real bones. However, the bone skeleton is approximately cut into 2D flake images. It is difficult to guarantee the integrity of the pore connectivity in bone. In addition, due to the inevitable errors of hierarchical image acquisition, there is substantial loss in 3D model fitting. It cannot guarantee the integrity of the structure, and it will result in poor mechanical properties. In addition, the surface morphology and pore distribution are out of effective control.

TABLE 3. Some simple TPMS constructed by trigonometric function.

TPMS	periodic trigonometric function
P	$\emptyset(r) = \cos(X) + \cos(Y) + \cos(Z) = 0$
D	$\emptyset(r) = \cos(X)\cos(Y)\cos(Z) - \sin(X)\sin(Y)\sin(Z) = 0$
G	$\emptyset(r) = \sin(X)\cos(Y) + \sin(Z)\cos(X) + \sin(Y)\cos(Z) = 0$
Rod	$\emptyset(r) = 4\cos(2X) + 4\cos(2Y) + 3 = 0$

III. MODELING METHOD

A. TPMS MODELING METHOD

TPMS is a minimal surface that exhibits periodicity in three independent directions in three-dimensional space. The surface has the characteristics of zero mean curvature and can be extended indefinitely in three periodic directions. It can provide a concise description for many physical structures, such as silicates and soluble colloids. As a pore forming unit, TPMS can realize the digital representation of a porous structure.

1) MATHEMATICAL EXPRESSIONS OF TPMS

There are many ways to generate TPMS coordinates, which have an exact parameterized form defined by the Weierstrass formula [30], [31], as shown in formula (8):

$$\begin{cases} x = Re\int_{\omega 0}^{\omega 1} e^{i\theta}\left(1-\omega^2\right)R(\omega)\,d\omega \\ y = Re\int_{\omega 0}^{\omega 1} e^{i\theta}\left(1+\omega^2\right)R(\omega)\,d\omega \\ z = Re\int_{\omega 0}^{\omega 1} e^{i\theta}(2\omega)R(\omega)\,d\omega \end{cases} \tag{8}$$

where ω represents a complex variable, θ is an angle called Bonnet, and $R(\omega)$ represents a function that varies with different surfaces. For P, D and G surfaces of TPMS, $R(\omega)$ can be expressed by the formula (9):

$$R(\omega) = \frac{1}{\sqrt{1 - 14\omega^4 + \omega^8}} \tag{9}$$

Compared with parametric TPMS, the approximate TPMS periodic surface is generally defined and can be expressed as shown in formula (10):

$$\emptyset(r) = \sum_{k=1}^{K} A_k cos\left[\frac{2\pi\,(h_k \cdot r)}{\lambda_k} + p_k\right] = C \tag{10}$$

where γ represents position vectors of Euclidean space, A_k represents amplitude factor, h_k is the kth grid vector in the reciprocal space, λ_k represents the periodic wavelength, p_k represents the phase offset, and C is a constant.

Approximate TPMS is formulated by implicit function, and each point on its surface has a constant value. The surface processing of this characteristic can be called the isosurface. Some approximate TPMS are listed in Table 3, where the standard value $\emptyset(r)_0 = 0$, $X = 2\pi x$, $Y = 2\pi y$, $Z = 2\pi z$.

2) STRUCTURING CURVED SURFACE

For an unclosed implicit surface defined by implicit function, one or more intersecting surfaces are need to define the structure of a closed surface. The main problem of structuring a curved surface is solving the intersection line of curved surface in three-dimensional space. For the intersection operation of an implicit surface and a parametric surface, a plane algebraic surface equation can be achieved by plugging the parametric function into the implicit function, and the problem can be solving by plane algebra theory. For the intersection operation of implicit surfaces, the solution is to parameterize one of the surfaces and refer to the above-mentioned method.

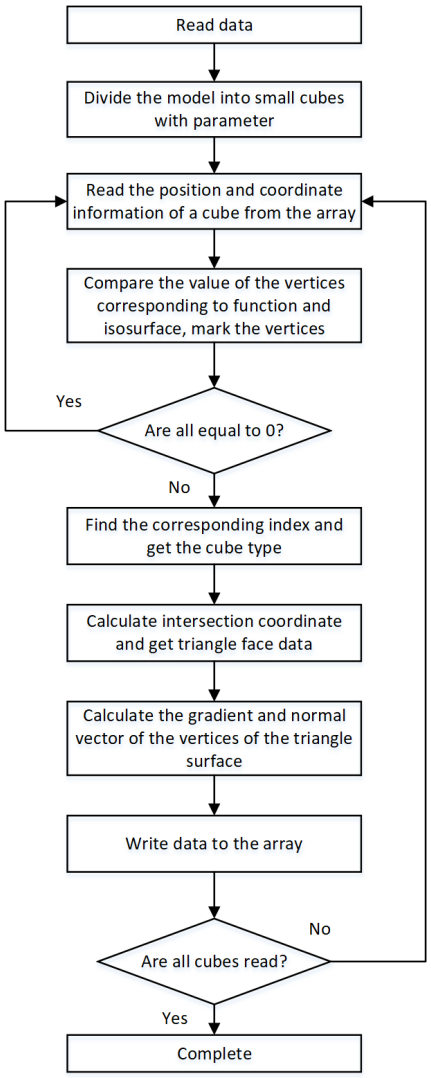

FIGURE 3. Algorithm flowchart of Marching Cubes.

3) SURFACE TRIANGULATION

With the parameter domain, the parametric surface can be constructed and triangulated by directly calculating the position of the point in surface. While the implicit surface does not have the parameter, it is hard to implement the similar transformation.

A Marching Cubes method was employed to triangulate the implicit surface. The basic principle of this method is that

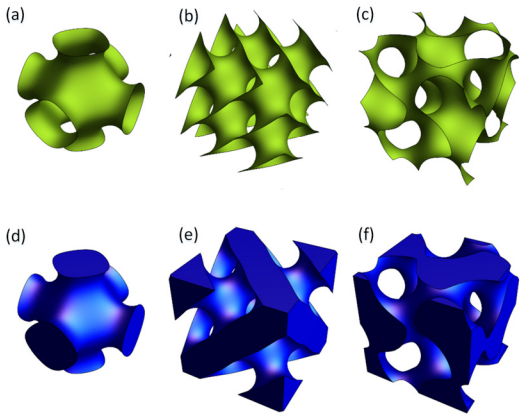

FIGURE 4. Triangulation of non-closed implicit surface: (a) P surface, (b) D surface, (c) G surface; triangulation of typical closed implicit surface: (d) P surface, (e) D surface, (f) G surface.

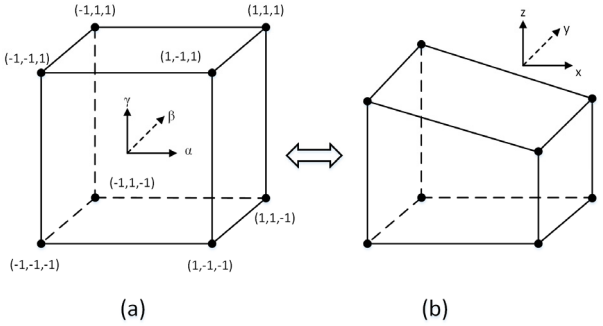

FIGURE 5. Mapping relation of the isoparametric element, (a) the natural (local) coordinate system, (b) the Descartes (global) coordinate system.

the intersection points of the isosurface and the hexahedron edge are connected in a certain way, and the new isosurface is approximated to represent the implicit surface. The algorithm flowchart of Marching Cubes is shown in Fig. 3.

The Marching Cubes method has the advantages of a simple algorithm and fast calculation speed. However, because of the inability to control the angle of the triangular patches, some triangular patches with very small or large angles will be generated, which results in the quality of the triangular patches and is not conducive to the generation of tetrahedral meshes.

After extracting the isosurface by the Marching Cube method, the corresponding STL (stereolithography) model can be conveniently extracted, and the STL model contains the triangular surface information of the external surface of the entity object. Moreover, the quality of the triangular patch has no real influence on the extraction and expression of the STL model. Therefore, the method has obvious advantages for porous structures or porous implants that need to be made by means of the additive manufacturing process.

The typical TPMS: P, D, G surfaces are triangulated and visualized separately, as shown in Fig. 4.

B. TRANSFORMATION OF PORE CELL BASED ON SHAPE FUNCTION

The TPMS unit is usually constructed in a hexahedron grid. After the mapping of the distribution rule of pore size to a hexahedral mesh model, we found that the unit in the bone scaffold model is a non-hexahedral cube. Therefore, in this paper, the shape function is used to transform the isoparametric elements of the fractal TPMS cell, which is mapped to the irregular hexahedral mesh. By the mapping relation of the function, a shape can be mapped to another shape, that is, the irregular geometry of one coordinate system can be mapped into a regular geometry of another coordinate system. Two coordinate systems are needed in the isoparametric element method, the natural (local) coordinate system and the Descartes (global) coordinate system. Irregular line segments, polygons and polyhedrons in the Descartes coordinate system can be converted into corresponding geometric shapes in the natural coordinate system. The Descartes coordinate system is represented by x, y and z, and the natural coordinate system is represented by a set of dimensionless parameters α, β, and γ that were within "1", and their boundary nodes correspond to points equal to -1 or 1 in the natural coordinate system.

The porous element, which is ruled by a regular hexahedron, is taken as the parent unit. It is mapped to the irregular element by coordinate transformation. The mapping must ensure that the points between the sub-unit and the parent-unit correspond one-to-one. That is, the compatibility of the coordinate transformation is satisfied. The mapping relation of the isoparametric element is shown in Fig. 5.

To transform the unit of shape rule in the natural coordinate system into irregular sub units in the Descartes coordinate system, a coordinate transformation must be set up to discretize the general shape solving domain. That can be expressed by formula (10):

$$\begin{pmatrix} x \\ y \\ z \end{pmatrix} = f\left(\begin{Bmatrix} \alpha \\ \beta \\ \gamma \end{Bmatrix}\right) \tag{11}$$

To realize the transformation mentioned above, the interpolation function is used to coordinate transformation, and the regular shape units in the natural coordinate system are transformed into irregular shapes in a Cartesian coordinate system:

$$\begin{pmatrix} x \\ y \\ z \end{pmatrix} = \sum_{i=1}^{8} N_i \begin{pmatrix} x_i \\ y_i \\ z_i \end{pmatrix} \quad i = 1, \cdots\cdots, 8 \tag{12}$$

where (x, y, z) are the coordinate of the unit point in the Cartesian coordinate system and (x_i, y_i, z_i) are the coordinate value of 8 nodes of hexahedron in the Cartesian coordinates. As a node shape function, Ni is an interpolation function expressed in natural coordinates, and can be obtained by the

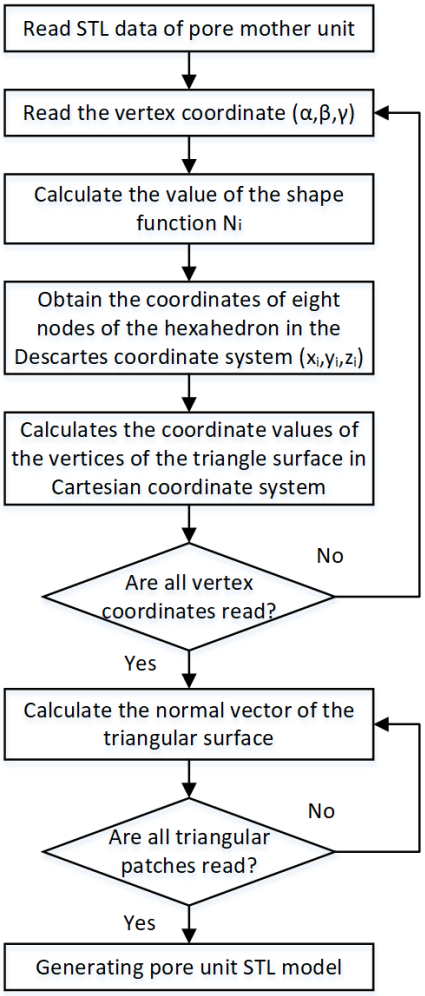

FIGURE 6. Flowchart of modeling sub-unit in space domain.

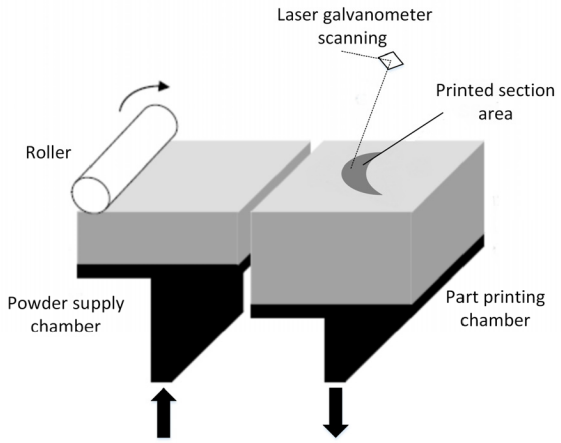

FIGURE 7. Schematic of the direct metal laser sintering process.

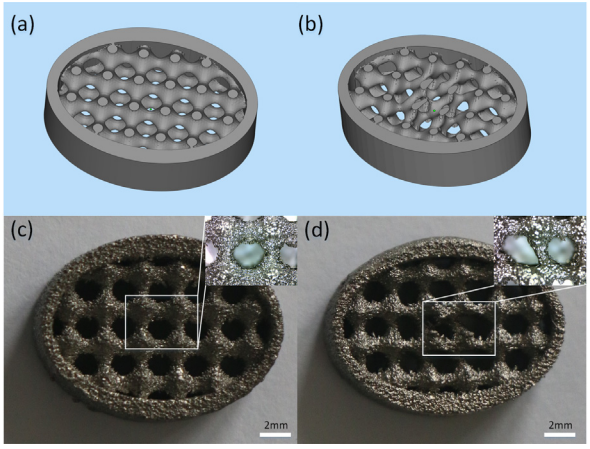

FIGURE 8. Modeling and fabrication of porous scaffold samples: (a) designed model with P-surface; (b) designed bionic model combining TPMS and shape function; (c) printed sample with P-surface; (d) printed bionic porous scaffold sample.

Lagrange interpolation method:

$$N_i = \frac{1}{8}(1+\alpha_i\alpha)(1+\beta_i\beta)(1+\gamma_i\gamma) \quad i = 1, \cdots\cdots, 8 \tag{13}$$

where $(\alpha_i, \beta_i, \gamma_i)$ is the coordinate point of node i in natural coordinate system and (α, β, γ) is the coordinate point of the inside entity in the natural coordinate system.

The essence of parametric modeling of porous structure is a kind of spatial structure characteristic that the pore forming units are arranged according to certain rules. Its performance is porous combinations with a single hole as a unit. Based on the TPMS construction algorithm, the pore cell modeling and parameter adjustment can be realized, and then the location and the spatial orientation of the pore cell can be controlled according to the structure distribution law. The flowchart of modeling sub-unit in space domain is shown in Fig. 6.

IV. BIONIC POROUS SCAFFOLD CONSTRUCTION

The rat femur was employed as the studied object, and the digital modeling of the porous structure was carried out through the research and statistics of the distribution rules of the structural parameters. The middle part of the rat femoral bone section was set as the studied sample. Two-dimensional chromatogram images were obtained by Micro-CT scanner. The images were processed by a binarization and skeletonization algorithm. Based on it, the 3D model of trabecular bone was reconstructed. Through the application of the skeletonization algorithm, the distribution information of trabecular bone was studied, and the parameters distribution rule of the porous structure was extracted and counted. The distribution rule was used as the constraint of the control functions of the structural parameters, and the geometric model of the porous unit was constructed by combining the unit model of TPMS. Finally, the bionic porous scaffold model was built and was generated in STL format.

The sample model was fabricated on the EOS M290 (EOS GmbH Electro Optical Systems, Germany) that employs DMLS (direct metal laser sintering) technology. A schematic diagram of the DMLS process is shown in Fig. 7.

With porous scaffold model obtaining by TPMS method, the Ti6Al4V powder was placed in the supply chamber of the

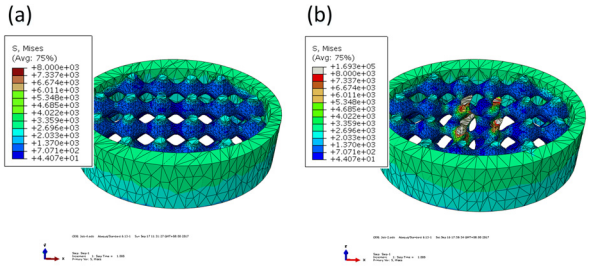

FIGURE 9. FEA results for the von Mises stress field of the two kinds of porous samples, sample with P-surface 1 (a), sample combining TPMS and shape function (b).

machine and spread evenly across the supplier and builder. During the printing process, the roller spread a layer of powder, 20-μm thick, onto the builder. The graphics trajectory was printed via a laser galvanometer scanning system, which sintered each layer of the powder on the builder. The process was looped until the samples were eventually formed, as shown in Fig. 8(cd).

The mechanical properties of the geometries shown in Fig.8 could be obtained from the FEA simulation. The loading conditions and boundary constraints are the same for the two scaffold samples. The FEA result for the von Mises stress field of the samples are shown in the Fig.9.

V. CONCLUSION

In this paper, a modeling method based on TPMS for the expression of surface morphology and pore size distribution of porous bone scaffold was proposed. Based on the analysis of porous structure of trabecular bone, the fractal TPMS pore forming unit was built with the combination of TPMS unit and fractal geometry, which describes the surface morphology of the pore structure. Through the hexahedral mesh split of the outer anatomy surface and the surrounding volume of the trabecular bone, the modeling of porous model with the controllable pore size distribution was realized with the adjustment of the internal hexahedral mesh vertex position of the model by the distribution of pore. The shape function of isoparametric transformation was used to map the fractal TPMS pore unit to hexahedral mesh, and the overall model of trabecular bone scaffold structure was finally designed. At last, the designed porous model was fabricated by 3D printing. The result verified the feasibility of the method.

REFERENCES

[1] Y. Fei, Y. Yao, and Q. Hu, "Generation and evaluation of porous structure of bionic bone scaffold," *J. Mech. Eng.*, vol. 47, no. 1, pp. 138–144, 2011.

[2] C. Yan, L. Hao, A. Hussein, and P. Young, "Ti–6Al–4V triply periodic minimal surface structures for bone implants fabricated via selective laser melting," *J. Mech. Behavior Biomed. Mater.*, vol. 51, pp. 61–73, Nov. 2015.

[3] P. Heinl, L. Müller, C. Körner, R. F. Singer, and F. A. Müller, "Cellular Ti–6Al–4V structures with interconnected macro porosity for bone implants fabricated by selective electron beam melting," *Acta Biomater.*, vol. 4, no. 5, pp. 1536–1544, 2008.

[4] W. Qinghui and X. Gang, "Modelling the microstructures of cancellous bone based on triply periodic minimal surface for tissue engineering," *J. Comput.-Aided Des. Comput. Graph.*, vol. 28, no. 11, pp. 1949–1956, 2016.

[5] W. Linbo and D. Jiandong, "Advances in fabrication methodology and technology of three-dimensional porous scaffolds for tissue engineering," *J. Funct. Polymers*, vol. 16, no. 1, pp. 91–96, 2003.

[6] D. J. Yoo, "Heterogeneous porous scaffold design for tissue engineering using triply periodic minimal surfaces," *Int. J. Precis. Eng. Manuf.*, vol. 13, no. 4, pp. 527–537, 2012.

[7] J. Shi, L. Zhu, Z. Li, J. Yang, and X. Wang, "A design and fabrication method for a heterogeneous model of 3D bio-printing," *IEEE Access*, vol. 5, pp. 5347–5353, 2017.

[8] S. Jianping, Y. Jiquan, L. Jingbo, and Z. Yufang, "The modeling and digital micro-droplet injection technology of heterogeneous material part," *J. Nanjing Normal Univ.*, vol. 12, no. 1, pp. 10–14, 2012.

[9] W. Malinauskas *et al.*, "3D microporous scaffolds manufactured via combination of fused filament fabrication and direct laser writing ablation," *Micromachines*, vol. 5, no. 4, pp. 839–858, 2014.

[10] S. Huang, Z. Chen, N. Pugno, Q. Chen, and W. Wang, "A novel model for porous scaffold to match the mechanical anisotropy and the hierarchical structure of bone," *Mater. Lett.*, vol. 122, no. 5, pp. 315–319, 2014.

[11] J. Kadkhodapour *et al.*, "The relationships between deformation mechanisms and mechanical properties of additively manufactured porous biomaterials," *J. Mech. Behavior Biomed. Mater.*, vol. 70, pp. 28–42, Jun. 2016.

[12] D.-J. Yoo and K.-H. Kim, "An advanced multi-morphology porous scaffold design method using volumetric distance field and beta growth function," *Int. J. Precision Eng. Manufact.*, vol. 16, no. 9, pp. 2021–2032, 2015.

[13] S. Tassani and G. K. Matsopoulos, "The micro-structure of bone trabecular fracture: An inter-site study," *Bone*, vol. 60, no. 3, pp. 78–86, 2014.

[14] L. Lv *et al.*, "Regional variations in trabecular morphological features of femoral head of patients with proximal femoral fractures," *J. Bionic Eng.*, vol. 12, no. 2, pp. 294–303, 2015.

[15] A. E. Jakus *et al.*, "Hyperelastic 'bone': A highly versatile, growth factor–free, osteoregenerative, scalable, and surgically friendly biomaterial," *Sci. Trans. Med.*, vol. 8, no. 358, p. 358ra127, 2016.

[16] D.-J. Yoo, "Computer-aided porous scaffold design for tissue engineering using triply periodic minimal surfaces," *Int. J. Precision Eng. Manuf.*, vol. 12, no. 1, pp. 61–71, 2011.

[17] N. Yang and K. Zhou, "Effective method for multi-scale gradient porous scaffold design and fabrication," *Mater. Sci. Eng., C*, vol. 43, pp. 502–505, Oct. 2014.

[18] D. Yoo, "Heterogeneous minimal surface porous scaffold design using the distance field and radial basis functions," *Med. Eng. Phys.*, vol. 34, no. 5, pp. 625–639, 2012.

[19] F. P. W. Melchels, K. Bertoldi, R. Gabbrielli, A. H. Velders, J. Feijen, and D. W. Grijpma, "Mathematically defined tissue engineering scaffold architectures prepared by stereolithography," *Biomaterials*, vol. 31, no. 27, pp. 6909–6916, 2010.

[20] N. Yang, C.-F. Du, S. Wang, Y. Yang, and C. Zhang, "Mathematically defined gradient porous materials," *Mater. Lett.*, vol. 173, pp. 136–140, Jun. 2016.

[21] N. Yang, Z. Quan, D. Zhang, and Y. Tian, "Multi-morphology transition hybridization CAD design of minimal surface porous structures for use in tissue engineering," *Comput.-Aided Des.*, vol. 56, no. 11, pp. 11–21, 2014.

[22] N. Yang, Y. Tian, and D. Zhang, "Novel real function based method to construct heterogeneous porous scaffolds and additive manufacturing for use in medical engineering," *Med. Eng. Phys.*, vol. 37, no. 11, pp. 1037–1046, 2015.

[23] D. A. Rajon *et al.*, "Image segmentation of trabecular spongiosa by visual inspection of the gradient magnitude," *Phys. Med. Biol.*, vol. 51, no. 18, pp. 4447–4467, 2006.

[24] L. Dan *et al.*, "The assessment of ectopic osteoinduction by bBMP using micro-CT," *J. Biomed. Eng. Res.*, vol. 29, no. 1, pp. 32–36, 2010.

[25] G.-H. Liu and J.-Y. Yang, "Image retrieval based on the texton co-occurrence matrix," *Pattern Recognit.*, vol. 41, no. 12, pp. 3521–3527, 2008.

[26] C. Shuyue, X. Yang, P. Yan, L. Mingzhi, Z. Huilong, and D. Linhong, "Quantitative characterization and analysis of the shape and distribution of microfilaments in rat airway smooth muscle cells," *J. Biomed. Eng. Res.*, vol. 3, pp. 152–157, Jun. 2015.

[27] P. J. F. Gandy *et al.*, "Nodal surface approximations to the P, G, D and IWP triply periodic minimal surfaces," *Chem. Phys. Lett.*, vol. 336, nos. 3–4, pp. 187–195, 2001.

[28] Y. Wang, "Periodic surface modeling for computer aided nano design," *Comput.-Aided Des.*, vol. 39, no. 3, pp. 179–189, 2007.

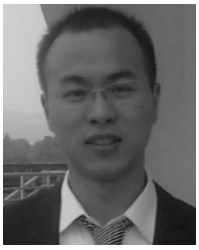

JIANPING SHI received the B.S. degree in mechanical engineering and the M.S. degree in electronic engineering from Nanjing Normal University, China, in 2010 and 2013, respectively. He is currently pursuing the Ph.D. degree with Southeast University. He is currently a Researcher with the Jiangsu Key Laboratory for 3-D Printing Equipment and Manufacturing. His research interests include 3-D printing methods and 3-D bio-printing for tissue engineering.

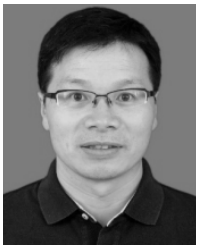

JIQUAN YANG received the B.S. degree in mechanical engineering and the Ph.D. degree in instrument science and technology from the Nanjing University of Science and Technology, China. He is currently a Professor at the Jiangsu Key Laboratory for 3-D Printing Equipment and Manufacturing, Nanjing Normal University. His research interests include 3-D printing.

LIYA ZHU received the B.S. degree from the Wuhan University of Technology, and the Ph.D. degree from the Nanjing University of Aeronautics and Astronautics, China. She is currently a Lecturer at the Jiangsu Key Laboratory for 3-D Printing Equipment and Manufacturing, Nanjing Normal University. Her research interests include 3-D bio-printing for tissue engineering.

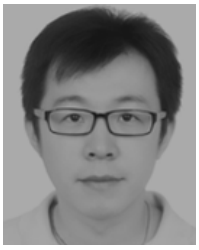

LAN LI received the B.S. degree in specialty of Chinese medicine in 2011, and the M.S. degree in electronic engineering from Nanjing University, China, in 2014. He is currently pursuing the Ph.D. degree with Southeast University. His research interests include 3-D printing methods and 3-D bio-printing for tissue engineering.

ZONGAN LI received the B.S. degree in mechanical engineering and the Ph.D. degree in instrument science and technology from the Nanjing University of Science and Technology, China, in 2009 and 2015, respectively. He is currently a Post-Doctoral Researcher at Southeast University. His research interests include developing 3-D model reconstruction software based on computed tomography images and 3-D bio-printing for tissue engineering.

XINGSONG WANG received the B.S. and M.S. degrees from Zhejiang University, Hangzhou, China, in 1991, and the Ph.D. degree from Southeast University, Nanjing, China, in 2000. He is currently a Full Professor with the School of Mechanical Engineering and the Department Head of the Department of Mechatronics, Southeast University. His current research interests include control theory with applications in precision computer numerical control machine tools, advanced mechatronics with applications in biomedical engineering, and tendon-sheath transmission theory with applications in rescue robots.